



Showcasing research from Professor Kulak's laboratory, Institute of Chemistry, University of Potsdam, Brandenburg, Germany.

A sodium ion-selective photosensitizer: dibrominated F-BODIPY as a fluorescence imaging and therapeutic agent

A photosensitizer, a benzo-15-crown-5 functionalized F-BODIPY dye, detects sodium with high selectivity, fast response, and bright, photostable fluorescence. Its signal and singlet oxygen generation are boosted by the elevated sodium levels as e.g. found in malignant cells, enabling precise tumour imaging. Upon light activation, the photosensitizer could selectively kill cancer cells, combining diagnostic power with therapeutic action. This dual functionality positions the photosensitizer as a promising agent for photodynamic cancer therapies.

Image reproduced by permission of Mazen Al Akrami from *Phys. Chem. Chem. Phys.*, 2025, **27**, 24178.

Cover image generated by iStock/Getty Images AI image generator.

As featured in:



See Thomas Schwarze, Nora Kulak *et al.*, *Phys. Chem. Chem. Phys.*, 2025, **27**, 24178.



Cite this: *Phys. Chem. Chem. Phys.*,  
2025, 27, 24178

# A sodium ion-selective photosensitizer: dibrominated F-BODIPY as a fluorescence imaging and therapeutic agent

Thomas Schwarze, \*<sup>a</sup> Mazen Al Akrami,<sup>a</sup> Julian Heinrich, <sup>a</sup> Vinja Hergl,<sup>a</sup>  
Eric Sperlich, <sup>a</sup> Alexandra Kelling,<sup>a</sup> Tobias Sprenger,<sup>ab</sup> Nicolas Jahn, <sup>a</sup>  
Tillmann Klamroth <sup>a</sup> and Nora Kulak \*<sup>a</sup>

Herein, we report that the production of singlet oxygen ( $^1\text{O}_2$ ) is exclusively regulated by sodium ions in aqueous solution by the use of a  $\text{Na}^+$ -selective photosensitizer (PS), a 2,6-dibrominated F-BODIPY dye equipped with benzo-15-crown-5. The PS showed an enhanced fluorescence quantum yield ( $\Phi_f$ ) and an enhanced singlet oxygen quantum yield ( $\Phi_\Delta$ ) in the presence of  $\text{Na}^+$ . A detailed theoretical study uncovered the underlying photophysical pathways which are responsible for both functional characteristics of the PS, therapeutic and  $\text{Na}^+$  imaging properties.

Received 18th August 2025,  
Accepted 20th September 2025

DOI: 10.1039/d5cp03172a

[rsc.li/pccp](http://rsc.li/pccp)

## 1. Introduction

Photodynamic therapy (PDT) is a non-invasive and very powerful method to kill cancer cells by singlet oxygen ( $^1\text{O}_2$ ) generated through light and a photosensitizer (PS).<sup>1,2</sup> Several PSs, mainly porphyrin derivatives are approved for the PDT treatment for different types of cancer such as skin, lung, bladder, and breast cancer.<sup>3</sup> In malign breast cancer cells the pH value can be more acidic and the  $\text{Na}^+$  level is up to five times higher than in benign cells (raising from around 20 mM to over 100 mM  $\text{Na}^+$ ).<sup>4</sup> A very powerful and non-invasive but costly technique to visualise  $\text{Na}^+$  in the human body is based on magnetic resonance imaging (MRI) of  $^{23}\text{Na}$ .<sup>5</sup> A more cost-effective method to image  $\text{Na}^+$  *in vivo* is the use of fluorescence spectroscopy.<sup>6,7</sup> For precise identification and targeted light irradiation of tumor tissue, a fluorescence imaging-guided PDT is very helpful.<sup>8,9</sup> A further class of promising triplet PSs for PDT are based on boron-dipyrromethene (BODIPY) dyes,<sup>10–12</sup> when for instance substituted in 2,6-position with heavy atoms such as iodine<sup>13–15</sup> or bromine.<sup>16</sup> Two decades ago, the group of Akkaya *et al.* reported on 2,6-dibromo-substituted F-BODIPYs as triplet PSs to efficiently produce  $^1\text{O}_2$ .<sup>16</sup> Further, O'Shea *et al.* published a while ago, that the  $^1\text{O}_2$  generation rate can be regulated by protons.<sup>17</sup> There, a photoinduced electron transfer (PET) is blocked by protonation of an amine donor.<sup>17</sup> Moreover, in a pioneering work Akkaya *et al.* showed that a PS consisting of

2,6-diiodo- and 3,5-dipyridylethenyl-substituted F-BODIPY equipped in *meso*-position with a benzo-15-crown-5 can modulate and enhance  $^1\text{O}_2$  production by both  $\text{H}^+$  and  $\text{Na}^+$  in acetonitrile (ACN).<sup>18</sup> Meanwhile, some factors that control the  $^1\text{O}_2$  efficiency have been uncovered such as pH, light, hydrogen peroxide, nucleic acids, proteins *etc.*<sup>18–21</sup>

In a recent study, we reported on a benzo-15-crown-5-equipped F-BODIPY dye **1a** (Fig. 1) for a reliable fluorescence detection of  $\text{Na}^+$  in the pH range from 3 to 10 by fluorescence enhancement caused by an off-switching of a PET by  $\text{Na}^+$  in aqueous solution.<sup>22</sup> Herein, we now report on a detailed experimental and theoretical study of the regulation of  $^1\text{O}_2$  exclusively by  $\text{Na}^+$  and the fluorescence sensing of  $\text{Na}^+$  by a PS in ACN and aqueous solution. Our overriding goal is to design a PS which shows an enhanced  $^1\text{O}_2$  production as well as an enhanced fluorescence response only in malign, but not in benign tissue. As a trigger we selected the enhanced  $\text{Na}^+$  level in breast cancer cells. By fine tuning the  $\text{Na}^+$  complexing abilities of the  $\text{Na}^+$ -responsive PS (dissociation constant  $K_d$ ) we aimed to manipulate the  $^1\text{O}_2$  evolution and fluorescence response. We designed PS **1** to be both, a therapeutic and an imaging agent regulated by the enhanced  $\text{Na}^+$  level in tumor tissue. PS **1** is a combination of the photostable triplet PS **2**,<sup>23</sup> a 2,6-dibromo-substituted F-BODIPY dye, and the pH-stable and  $\text{Na}^+$ -selective binding unit **3**, benzo-15-crown-5<sup>24</sup> (Fig. 1).

## 2. Results and discussion

A bromination at positions 2 and 6 of the F-BODIPY **1a**<sup>22</sup> with *N*-bromosuccinimide (NBS) yielded the novel PS **1** in a

<sup>a</sup> Institute of Chemistry, University of Potsdam, 14476 Potsdam, Germany.  
E-mail: [schwarth@uni-potsdam.de](mailto:schwarth@uni-potsdam.de), [nora.kulak@uni-potsdam.de](mailto:nora.kulak@uni-potsdam.de)

<sup>b</sup> Faculty of Medicine, Health and Medical University (HMU), 14471 Potsdam, Germany



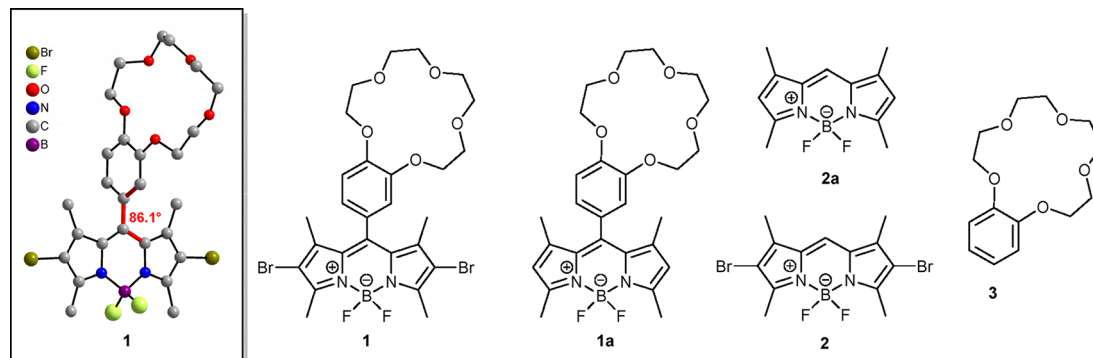


Fig. 1 Studied  $\text{Na}^+$ -selective 2,6-dibrominated F-BODIPY PS **1** (left: molecular structure obtained from XRD) and reference compounds **1a**, **2**, **2a** and **3**. H atoms are omitted for clarity.

moderate yield of 47%.<sup>25</sup> As references, the F-BODIPYs **2** and **2a** without benzo-15-crown-5 moiety were synthesized as described.<sup>22,26</sup> Benzo-15-crown-5 (**3**) is commercially available. The novel PS **1** was characterized by  $^1\text{H}$  and  $^{13}\text{C}$  NMR spectroscopy as well as electrospray ionization mass spectrometry.<sup>25</sup> The molecular structure of **1** was confirmed by X-ray analysis (Fig. 1).<sup>25</sup> Single crystals of **1** were obtained by slow solvent evaporation (ethyl acetate/hexane, v/v, 1/1). At first, we recorded UV/Vis absorption spectra of **1** and **2** in ACN (Fig. S2a). The absorption spectra of **1** and **2** are very similar, in the range from 350 nm to 550 nm, to each other. They show the most intense absorption band ( $S_0$  to  $S_1$  transition) with a local maximum ( $\lambda_{\text{max}}$ ) at about 525 nm (vibronic 0–0 state) with a shoulder at about 490 nm (vibronic 0–1 state).<sup>27</sup> The molar extinction coefficients ( $\epsilon_\lambda$ ) at  $\lambda_{\text{max}}$  for **1** ( $77\,000\ \text{M}^{-1}\ \text{cm}^{-1}$ ) and **2** ( $75\,000\ \text{M}^{-1}\ \text{cm}^{-1}$ ) in ACN are comparable to each other, suggesting that the phenylic substituent in *meso*-position of the F-BODIPY in **1** does not significantly extend the  $\pi$ -electron system of the F-BODIPY chromophore. As found in the molecular structure of **1** the phenyl ring is almost orthogonal to the planar F-BODIPY core (dihedral angle  $86.1^\circ$ , Fig. 1) which electronically decouples the F-BODIPY from the benzo-15-crown-5. Then, we recorded UV/Vis absorption spectra of **1** and **2** ( $c_{\text{dye}} = 10^{-5}\ \text{M}$  and  $10^{-6}\ \text{M}$ , respectively) in different ACN/water mixtures and found a good solubility of **1** and **2** up to a ACN/water mixture of 1/9 (v/v) (Fig. S2c–f), but **2** showed a blue shift of  $\lambda_{\text{max}}$  when the water amount was increased (Fig. 2d and f).<sup>25</sup> Thus, **2** is only an appropriate spectroscopic reference compound for **1** in ACN. Moreover, to ensure complete solubility of **1**, we decided for further investigation to use as an aqueous solution an ACN/water mixture of 1/3 (v/v). Further, the fluorescence emission maxima of **1** and **2** ( $c = 10^{-6}\ \text{M}$ ) were also very similar to each other in ACN (539 nm (**1**) and 540 nm (**2**)) (Fig. S6a), but their fluorescence quantum yields ( $\Phi_f$ ) differ from each other ( $\Phi_f = 0.010$  (**1**),  $\Phi_f = 0.207$  (**2**)).<sup>25</sup> The low  $\Phi_f$  value of **2** is caused by a heavy atom quenching effect which is typical for a triplet PS.<sup>28</sup> Probably, in **1** an additional quenching process, such as in **1a** ( $\Phi_f = 0.258$ <sup>22</sup> in ACN(**1a**)), a reductive PET from the benzo-15-crown-5 (electron donor) to the excited and decoupled 2,6-dibrominated F-BODIPY core (electron acceptor)



Fig. 2 Fluorescence intensity ( $I_f$ ) of **1** ( $c = 10^{-6}\ \text{M}$ ,  $\lambda_{\text{ex}} = 500\ \text{nm}$ ) in the presence of different  $\text{Na}^+$  concentrations (a) in ACN and (b) in ACN/water, (v/v, 1/3). Fluorescence quantum yields ( $\Phi_f$ ) (black) and singlet oxygen quantum yields ( $\Phi_\Delta$ ) (red) of **1** in the presence of different  $\text{Na}^+$  concentrations (c) in ACN and (d) in ACN/water (v/v, 1/3). Photographs under UV light (366 nm) of **1** ( $c = 10^{-6}\ \text{M}$ ) in the presence of different  $\text{Na}^+$  concentrations (e) in ACN and (f) in ACN/water (v/v, 1/3).

occurs.<sup>29–31</sup> Solvent effects on the  $\Phi_f$  values for **1** are found because the reductive PET in **1** is more favorable in polar solvents (Table S3).<sup>25</sup> The low  $\Phi_f$  values of **1**, **1a** and **2** in polar solvents make them suitable candidates as PS to produce efficiently  $^1\text{O}_2$  in ACN and aqueous solution. Then we monitored the  $^1\text{O}_2$  production by recording the absorbance of **1**, 3-diphenylisobenzofuran (DPBF) as a singlet oxygen scavenger at 410 nm in ACN, aqueous solution (ACN/water, v/v, 1/3) and 1,4-dioxane/dimethyl sulfoxide (v/v, 99/1).<sup>25</sup> The following singlet oxygen quantum yields ( $\Phi_\Delta$ ) were calculated:  $0.199 \pm 0.010$  for **1**,  $0.239 \pm 0.010$  for **1a** and  $0.495 \pm 0.092$  for **2** in ACN,  $0.527 \pm 0.012$  for **1**,  $0.048 \pm 0.002$  for **1a** and  $0.521 \pm 0.014$  for **2** in 1,4-dioxane/dimethyl sulfoxide (v/v, 99/1) as well as for **1**  $0.126 \pm 0.003$  in aqueous solution (ACN/water, v/v, 1/3). The triplet PS **2** generates more  $^1\text{O}_2$  than **1** and **1a** in ACN and exhibits very similar  $\Phi_\Delta$  values in both polar and non-polar



solvents. The intersystem crossing (ISC) process in **2**, caused by the heavy atom effect of the two bromine atoms, results in a well populated triplet state ( $T_1$ ), which is less dependent on the solvent polarity.<sup>25,32</sup> The PS **1** exhibits a similar  $\Phi_\Delta$  value in non-polar environments to that of **2**, and shows a higher  $\Phi_\Delta$  value compared to its behaviour in more polar solvents. In contrast, **1a** displays the opposite trend: it has a higher  $\Phi_\Delta$  value in polar solvents and a lower  $\Phi_\Delta$  value in non-polar environments. In **1**, two deactivation pathways from the  $S_1$  state to the  $T_1$  state are conceivable. Firstly, ISC, which is typical for heavy atom containing triplet PS,<sup>13,16,28</sup> and secondly, a spin-orbit charge-transfer (SOCT)-ISC process, which predominates in heavy atom-free triplet PS,<sup>33–36</sup> such as PET-based PS, where a charge-separated  $^1CT$  state is formed and stabilized in polar solvents.<sup>34</sup> In general, the SOCT-ISC proceeds much faster than the ordinary ISC between  $\pi$  to  $\pi^*$  states.<sup>37</sup> For the heavy atom-free triplet PS **1a**, we observed a higher  $\Phi_\Delta$  value in polar solvents compared to the reference F-BODIPY **2a** ( $\Phi_\Delta = 0.09$  in ACN).<sup>38</sup> This enhancement is likely due to a SOCT-ISC process facilitated by the polar environment. Moreover, we observed similar  $\Phi_\Delta$  values for **1** and **1a** in ACN, indicating that in both PS, the SOCT-ISC is likely the predominant pathway from the  $^1CT$  state to the  $T_1$  state, in **1** the SOCT-ISC process likely predominates in polar solvents whereas conventional ISC is more dominant in non-polar environments.<sup>25</sup>

Further, we recorded UV/Vis absorption spectra of **1** ( $c = 10^{-5}$  M) in the presence of  $Na^+$  in ACN and in an ACN/water mixture of 1/3 (v/v) (Fig. S3a and b). The absorption at 540 nm ( $\lambda_{max}$ ) is nearly unaffected by  $Na^+$ . The complexation of  $Na^+$  within the benzo-15-crown-5 in **1** can be observed by an enhanced blue-shift of the  $\pi \rightarrow \pi^*$  transition from around 280 nm to 270 nm, (Fig. S3a and b) which is typical for cation complexation of benzo-crown ethers.<sup>39</sup> Then, we measured the influence of  $Na^+$  on the fluorescence intensity ( $I_f$ ),  $\Phi_f$  and  $\Phi_\Delta$  of **1** in ACN and aqueous solution (ACN/water, v/v, 1/3). The  $I_f$  of **1** is enhanced with increasing  $Na^+$  concentrations in ACN and aqueous solution (ACN/water, v/v, 1/3) (Fig. 2a and b). The relative course of both titration curves ( $\lambda_{em} = 540$  nm, Fig. S7b and d) is similar but the maximum FE is reached at different  $Na^+$  concentrations, in ACN at 5 mM and in aqueous solution (ACN/water, v/v, 1/3) at 2 M, respectively. The fluorescence enhancement factor (FEF) induced by  $Na^+$  in ACN is  $11.6 \pm 0.1$  at 5 mM  $Na^+$  and in ACN/water (v/v, 1/3) is  $9.1 \pm 0.5$  at 2 M  $Na^+$ , respectively. We also observed an enhancement of the  $\Phi_f$  values of **1** in the presence of different  $Na^+$  concentrations in ACN and aqueous solutions (ACN/water, v/v, 1/3) (Fig. 2c, d and Tables S4, S5). Here, we observed the highest  $\Phi_f$  value for **1** at 5 mM  $Na^+$  in ACN ( $\Phi_f = 0.132 \pm 0.004$ ) and in aqueous solution (ACN/water, v/v, 1/3) at 2000 mM  $Na^+$  ( $\Phi_f = 0.108 \pm 0.016$ ). Probably, the FE is caused by blocking the PET process in **1** by  $Na^+$ , as also found for **1a** +  $Na^+$ .<sup>22</sup>  $Na^+$  raises the oxidation potential of the PET electron donor benzo-15-crown-5 in ACN and aqueous solution.<sup>40</sup> Therefore, the reductive PET process in **1** +  $Na^+$  becomes more unlikely as expressed by the Rehm–Weller equation.<sup>30</sup> Moreover, we also determined an enhanced  $\Phi_\Delta$  value for **1** in the presence of different  $Na^+$  concentrations in both ACN and aqueous solution (ACN/water, v/v, 1/3), (Fig. 2c, d and Tables S1, S2). We

also observed the highest  $\Phi_\Delta$  value for **1** at 5 mM  $Na^+$  in ACN ( $\Phi_\Delta = 0.367 \pm 0.007$ ) and in aqueous solution (ACN/water, v/v, 1/3) at 2000 mM  $Na^+$  ( $\Phi_\Delta = 0.185 \pm 0.006$ ). Moreover, we determined for **1a** + 5 mM  $Na^+$  a  $\Phi_\Delta$  value of  $0.137 \pm 0.006$  in ACN which is close to the  $\Phi_\Delta$  value of 0.09 of **2a** in ACN.<sup>38</sup> Overall, we observed for **1** an enhancement of  $I_f$ ,  $\Phi_f$  and  $\Phi_\Delta$  by  $Na^+$  and for **1a** an enhancement of  $I_f$  and  $\Phi_f$  but a reduction of  $\Phi_\Delta$  by  $Na^+$  in polar solvents. Further, we calculated the limit of detection (LOD) from the fluorescence titration data of **1** +  $Na^+$  (LOD =  $3\sigma/m$ ) in ACN and aqueous solution (ACN/water, v/v, 1/3).<sup>25</sup> The PS **1** shows a lower sensitivity towards  $Na^+$  in ACN with a LOD of  $(9.45 \pm 0.6)$   $\mu$ M as in aqueous solution (ACN/water, v/v, 1/3) ( $11.5 \pm 1.1$ ) mM, respectively (Fig. S9a and b). We also found a good linear relationship between the fluorescence intensity of **1** +  $Na^+$  in ACN and aqueous solution (ACN/water, v/v, 1/3) (from 0 mM to 0.14 mM  $Na^+$ ,  $R^2 = 0.9966$  (ACN), from 0 mM to 100 mM  $Na^+$ ,  $R^2 = 0.9992$  (ACN/water, v/v, 1/3), Fig. S9a and b) at 540 nm, respectively. More importantly, we calculated from the fluorescence intensity changes of **1** +  $Na^+$  their dissociation constants ( $K_d$ ) in ACN and in aqueous solution (ACN/water, v/v, 1/3) resulting in  $K_d$  values of  $(0.16 \pm 0.02)$  mM and  $(209 \pm 5)$  mM, respectively.<sup>25</sup> The latter  $K_d$  value of **1** +  $Na^+$  in aqueous solution is biologically relevant, since it is close to the  $Na^+$  level in malign breast cancer cells.<sup>4</sup> The  $K_d$  value of **1** +  $Na^+$  is significantly lower in ACN than in aqueous solution caused by the fact that a solvent like ACN that does not coordinate strongly with  $Na^+$  and a complexation of  $Na^+$  within the benzo-15-crown-5 is less hampered. In addition to it, the slopes of the plots for **1** +  $Na^+$  ( $\log(c_{Na^+})$  vs.  $\log[(I_f - I_{fmin})/(I_{fmax} - I_f)]$ ) in ACN and aqueous solution (ACN/water, v/v, 1/3) were nearly 1 (Fig. S8a and b),<sup>25</sup> suggesting a 1 : 1 binding ratio between  $Na^+$  and **1**. Moreover, to elucidate the binding stoichiometry between **1** with  $NaClO_4$  in solution, we carried out  $^1H$  NMR experiments in  $CD_3CN$  (Fig. S12).<sup>25</sup> Thus, a 1 : 1 binding stoichiometry of **1** with  $NaClO_4$  was confirmed by a Job's plot analysis (Fig. S13).<sup>25</sup> We observed a downfield shift of the benzo-15-crown-5 protons until one equivalent  $NaClO_4$  in the  $^1H$  NMR spectra of **1** (Fig. S12) assuming that  $Na^+$  is coordinated within the benzo-15-crown-5 in **1**.

EPR experiments were carried out with 2,2,6,6-tetramethyl piperidine (TEMP) as a  $^1O_2$  specific spin-trap agent.<sup>25</sup> It was added to **1** and **1** + 5 mM  $NaClO_4$ , and a strong EPR signal of 2,2,6,6-tetramethylpiperidinyloxyl (TEMPO) was observed after light irradiation in ACN (Fig. S30). We found for **1** + 5 mM  $NaClO_4$  a two times higher intensity of the TEMPO signal at 336.58 mT than for **1** indicating that in the presence of  $Na^+$  more  $^1O_2$  is produced.

We further investigated the influence of varying aqueous pH values on the fluorescence performance of **1**.<sup>25</sup> **1** shows very stable invariant fluorescence emission signals in the pH value range from 3.04 to 10.04 (Fig. S11a). Moreover, we observed for **1** in ACN and aqueous solution (ACN/water, v/v, 1/3) over a time period of 360 min a relatively photostable fluorescence signal at 540 nm (Fig. S11b) meaning that the photobleaching of **1** is negligible. To verify selectivity of **1** for  $Na^+$  towards other important biological cations such as  $Li^+$ ,  $K^+$ ,  $NH_4^+$ ,  $Mg^{2+}$ ,  $Ca^{2+}$ ,  $Mn^{2+}$ ,  $Fe^{3+}$ ,  $Cu^{2+}$  and  $Zn^{2+}$ , we measured the fluorescence



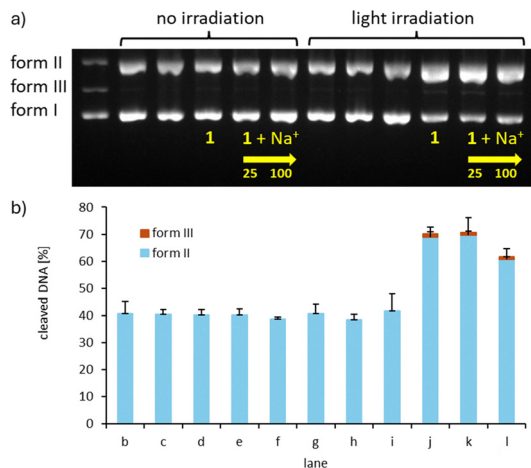


**Fig. 3** (a) Nuclease activity towards plasmid DNA pBR322 ( $0.025 \mu\text{g} \mu\text{L}^{-1}$ ) of PS **1** ( $c = 200 \mu\text{M}$ ) in Tris buffer (5 mM, pH 7.4) w/o NaCl (25 or 100 mM). Samples in lanes g–l were incubated under irradiation by green light for 50 min whereas samples in lanes a–f were not irradiated. Lane a: DNA ladder (form I, II and III), lane b + g: DNA reference, lanes c + i: 100 mM NaCl, lanes d + j: **1**, lanes e + k: **1** + 25 mM NaCl, lanes f + l: **1** + 100 mM NaCl, lane h: 25 mM NaCl. (b) Visualization of the extent of DNA cleavage in percent with standard deviation as error bars.

intensities in the presence of these cations at their respective concentrations that are biologically relevant in aqueous solution (ACN/water, v/v, 1/3).<sup>25</sup> The fluorescence performance of **1** is only slightly impacted (Fig. S10), showing that **1** is a  $\text{Na}^+$ -selective fluorescent imaging tool.

Moreover, we tested the DNA cleavage activity of **1** ( $c = 200 \mu\text{M}$ ) with plasmid DNA at pH 7.4 with or without green light irradiation in the absence or presence of NaCl (Fig. 3) or  $\text{NaClO}_4$  (Fig. S28). Degradation of supercoiled DNA (form I) to open-circular/nicked (form II) and linear DNA (form III) was monitored *via* gel electrophoresis.<sup>25</sup> Under green light irradiation, we observed DNA cleavage by **1** (lane j) forming 69% DNA form II (single-strand breaks) and even 1% form III (double-strand breaks). When the sample was not irradiated, no cleavage activity of **1** was observed (lane d about 40% form II). Surprisingly, the cleavage activity is not enhanced by NaCl (lanes k and l, Fig. 3) or  $\text{NaClO}_4$  (Fig. S28). Probably, the stabilisation of the negatively charged DNA

double helix (phosphate backbone) by  $\text{Na}^+$  due to electrostatic interactions<sup>41</sup> results in a lower DNA cleavage activity of **1**.

Further, we crystallized **1** with  $\text{NaClO}_4$  in a molar ratio of 1 : 1 from a chloroform/acetonitrile (v/v, 3/1) mixture to get more insights on the binding characteristics of  $\text{Na}^+$  within **1**. X-ray analysis provided the molecular structure of the  $\text{Na}^+$  complex  $[\text{Na}(\mathbf{1})(\text{ClO}_4)]$  (Fig. 4).  $\text{Na}^+$  is mainly coordinated by the five oxygen atoms of the benzo-15-crown-5 in **1** and shows a good fit-in-size into the cavity (Fig. 4a). Notably, the two symmetry-equivalent bridging perchlorate anions are disordered which influences the total number of coordination bonds of the  $\text{Na}^+$  (Fig. S23 and S24). We also found an electronic decoupling of the F-BODIPY from the  $\text{Na}^+$  complexed benzo-15-crown-5 unit because in the molecular structure of  $[\text{Na}(\mathbf{1})(\text{ClO}_4)]$  the phenyl ring is almost orthogonal to the planar F-BODIPY core (dihedral angle  $82.2^\circ$ , Fig. 4b).

Complementary to the experiments, we performed (time-dependent) density functional theory [(TD)-DFT] and singlet/triplet spin-orbit coupling (SOC) calculations of **1**, a dibromine-free F-BODIPY dye **1a** and **2** at the B3LYP/def2-TZVP level of theory<sup>43–45</sup> in ORCA 6.0.<sup>25,46</sup> The bright  $S_1$  state of **1** in Fig. 5c is given by a local transition on the BODIPY part from  $\text{MO}_{\text{Dye}}$  to the LUMO, while the optically dark  $^1\text{CT}$  state shows strong charge transfer character from  $\text{MO}_{\text{CT}}$  to the LUMO. We find that the addition of  $\text{Na}^+$  leads to an energetic stabilization of the  $\text{MO}_{\text{CT}}$ , while the two BODIPY-localized MOs remain mostly unaffected as shown in Fig. 5d due to the greater spatial distance to the crown ether part of **1**. The excitation energy of the  $^1\text{CT}$  state is thus increased relative to the bright  $S_1$  state after  $\text{Na}^+$  complexation in agreement with the reported experimental findings.<sup>25</sup> Furthermore, bromination leads to a one order of magnitude increase in the computed singlet/triplet SOCs of **1** compared to **1a** due to the heavy-atom effect of the bromine atoms.<sup>25</sup>

Overall, the fluorescence quenching observed for **1** is likely due to a reductive PET process. In polar solvents, a  $^1\text{CT}$  state is formed and stabilized, and its conversion to  $T_1$  state *via* a SOCT-ISC mechanism is probable. The resulting  $T_1$  state subsequently generates a moderate amount of  $^1\text{O}_2$  in polar solvents. Furthermore, we assume that  $\text{Na}^+$  interrupts the reductive PET process in **1** in polar solvents, leading to an increase in the energy of the  $^1\text{CT}$  state. As a result, population of the  $T_1$  state *via* ISC, facilitated by the heavy atoms (bromine), becomes more favourable and efficient, thereby restoring both fluorescence and  $^1\text{O}_2$  generation of the dibrominated F-BODIPY core ( $\Phi_f$  and  $\Phi_\Delta$  values of **2** in polar media). As a result we observed for **1** +  $\text{Na}^+$  higher  $\Phi_f$  and  $\Phi_\Delta$  values compared to **1** without  $\text{Na}^+$  (Fig. 5a and b). The latter can lead to degradation of DNA under irradiation (Fig. 3a and b). Moreover, we found for the dibromine-free F-BODIPY dye **1a** in the presence of  $\text{Na}^+$  also an enhanced  $\Phi_f$  value but a reduced  $\Phi_\Delta$  value in polar solvents. The presence of  $\text{Na}^+$  blocks the reductive PET process in **1a**, resulting in an elevation of the  $^1\text{CT}$  energy level. This effectively restores the fluorescence of the dibromine-free F-BODIPY core, where intersystem crossing (ISC) is considered highly unlikely (Fig. S34a and b). To the best of our knowledge, this is the first report that only a metal ion, here  $\text{Na}^+$ , regulates  $^1\text{O}_2$  evolution. The enhanced  $^1\text{O}_2$  production by  $\text{Na}^+$  can be useful to selectively kill malign cancer cells after

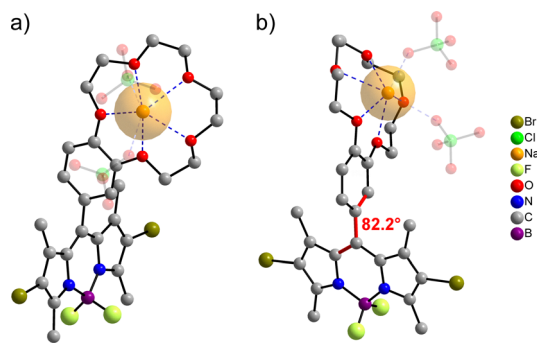


**Fig. 4** Molecular structure of  $[\text{Na}(\mathbf{1})\text{ClO}_4]$  with a space-filling model of Na (crystal radius<sup>42</sup> regarding coordination number). (a) Front view and (b) side view. H atoms are omitted for clarity.





Fig. 5 Jablonski diagram of the postulated mechanism of the photosensitized production of  $^1\text{O}_2$  in the PS **1** in polar solvents (a) without  $\text{Na}^+$  and (b) with  $\text{Na}^+$ . (c) Molecular orbitals (MOs) of **1** corresponding to the  $\text{S}_1$  and  $^1\text{CT}$  excited states (see further explanations in the text). (d) Relative MO energy level changes of **1** due to the addition of  $\text{Na}^+$ .

irradiation when the  $K_d$  value of the  $\text{Na}^+$ -selective PS fits to the  $\text{Na}^+$  levels in the cancer cells.

### 3. Conclusions

In summary, we synthesized the novel and  $\text{Na}^+$  selective PS **1** consisting of a benzo-15-crown-5 and a dibrominated F-BODIPY dye shows a fluorescence signal which is photostable and invariant to a wide pH value range from 3.04 to 10.04. Further, **1** is a fluorescent tool with high  $\text{Na}^+$  selectivity and  $\text{Na}^+$  sensitivity, fast  $\text{Na}^+$  response and the  $\text{Na}^+$  induced fluorescence enhancement is even recognizable with the naked eye after irradiation with UV light. Moreover, we observed higher  $\Phi_f$  and  $\Phi_\Delta$  values for **1** in the presence of  $\text{Na}^+$  in polar solvents. The  $K_d$  value of **1** +  $\text{Na}^+$  is  $(209 \pm 5)$  mM in aqueous solution and fits better to the  $\text{Na}^+$  level in malign cancer cells (around 100 mM  $\text{Na}^+$ ) than to benign cells (around 20 mM  $\text{Na}^+$ ).<sup>4</sup> PS **1** is a suitable therapeutic as well as a  $\text{Na}^+$  imaging agent. **1** could be a useful PS for cancer therapy because **1** could image tumorous tissue, and targeted light irradiation would selectively kill cancer cells through  $^1\text{O}_2$  generation. Currently, we are designing PSs applicable in PDT for a deeper tissue penetration by extending the  $\pi$ -system in position 2 and 5 of the F-BODIPY core to shift absorbance to the near-infrared (NIR) region.<sup>47</sup>

### Author contributions

Thomas Schwarze: conceptualization, methodology, investigation, formal analysis, writing – original draft; Mazen Al Akrami: investigation, data curation; Julian Heinrich: formal analysis, data curation; Vinja Hergl: investigation; Alexandra Kelling: formal analysis; Eric Sperlich: formal analysis, visualisation, methodology; Tobias Sprenger: formal analysis; Nicolas Jahn: formal analysis, visualisation; Tillmann Klamroth: supervision; Nora Kulak: funding acquisition, supervision, writing – review & editing.

### Conflicts of interest

The authors declare no conflict of interest.

### Data availability

The data supporting this article have been included as part of the supplementary information (SI). Supplementary information: synthesis, data from NMR, EPR, UV/Vis and fluorescence spectroscopy, cyclic voltammetry, single crystal X-ray diffraction, DNA cleavage experiments and DFT calculations. See DOI: <https://doi.org/10.1039/d5cp03172a>.

CCDC 2457233 and 2477061 contain the supplementary crystallographic data for this paper.<sup>48a,b</sup>

### Acknowledgements

The authors thank Matthias Hartlieb for providing access to a PhotoCube reactor (ThalesNano). The German Research Foundation (DFG) is acknowledged for funding within SFB 1636 (Project ID 510943930) for establishing EPR experiments under irradiation.

### Notes and references

- 1 Y. Allamyradov, J. ben Yosef, B. Annamuradov, M. Ateyeh, C. Street, H. Whipple and A. O. Er, *Photochemistry*, 2024, **4**, 434.
- 2 J. F. Algorri, M. Ochoa, P. Roldán-Varona and J. M. López-Higuera, *Cancers*, 2021, **13**, 4447.
- 3 A.-G. Niculescu and A. M. Grumezescu, *Appl. Sci.*, 2021, **11**, 3626.
- 4 R. Ouwerkerk, M. A. Jacobs, K. J. Macura, A. C. Wolff, V. Stearns, S. D. Mezban, N. F. Khouri, D. A. Bluemke and P. A. Bottomley, *Breast Cancer Res. Treat.*, 2007, **106**, 151.
- 5 L. O. Poku, M. Phil, Y. Cheng, K. Wang and X. Sun, *J. Magn. Reson. Imaging*, 2021, **53**, 995.



- 6 J. M. Dubach, E. Lim, N. Zhang, K. P. Francis and H. Clark, *Integr. Biol.*, 2011, **3**, 142.
- 7 O. Iamshanova, P. Mariot, V. Lehenkyi and N. Prevarskaya, *Eur. Biophys. J.*, 2016, **45**, 765.
- 8 J. P. Celli, B. Q. Spring, I. Rizvi, C. L. Evans, K. S. Samkoe, S. Verma, B. W. Pogue and T. Hasan, *Chem. Rev.*, 2010, **110**, 2795.
- 9 H. Luo and S. Gao, *J. Control. Release*, 2023, **362**, 425.
- 10 A. Kamkaew, S. H. Lim, H. B. Lee, L. V. Kiew, L. Y. Chung and K. Burgess, *Chem. Soc. Rev.*, 2013, **42**, 77.
- 11 Z. Mao, J. H. Kim, J. Lee, H. Xiong, F. Zhang and J. S. Kim, *Coord. Chem. Rev.*, 2023, **476**, 214908.
- 12 E. Bassan, A. Gualandi, P. G. Cozzi and P. Ceroni, *Chem. Sci.*, 2021, **12**, 6607.
- 13 T. Yogo, Y. Urano, Y. Ishitsuka, F. Maniwa and T. Nagano, *J. Am. Chem. Soc.*, 2005, **127**, 12162.
- 14 J. Piskorz, W. Porolnik, M. Kucinska, J. Dlugaszewska, M. Murias and J. Mielcarek, *ChemMedChem*, 2021, **16**, 399.
- 15 P. Rybczynski, A. Smolarkiewicz-Wyczachowski, M. Ziegler-Borowska, D. Kedziera, J. Piskorz, S. Bocian and A. Kaczmarek-Kedziera, *Int. J. Mol. Sci.*, 2021, **22**, 6735.
- 16 S. Atilgan, Z. Ekmekci, A. L. Dogan, D. Guc and E. U. Akkaya, *Chem. Commun.*, 2006, 4398.
- 17 S. O. McDonnell, M. J. Hall, L. T. Allen, A. Byrne, W. M. Gallagher and D. F. O'Shea, *J. Am. Chem. Soc.*, 2005, **127**, 16360.
- 18 S. Ozlem and E. U. Akkaya, *J. Am. Chem. Soc.*, 2009, **131**, 48.
- 19 S. Callaghan and M. O. Senge, *Photochem. Photobiol. Sci.*, 2018, **17**, 1490.
- 20 W. Wu, X. Shao, J. Zhao and M. Wu, *Adv. Sci.*, 2017, **4**, 1700113.
- 21 N. Kwon, H. Weng, M. A. Rajora and G. Zheng, *Angew. Chem., Int. Ed.*, 2025, **64**, e202423348.
- 22 T. Sprenger, T. Schwarze, H. Müller, E. Sperlich, A. Kelling, H.-J. Holdt, J. Paul, V. Martos Riaño and M. Nazaré, *Chem-PhotoChem*, 2023, **7**, e202200270.
- 23 E. N. Nuraneeva, E. V. Antina, G. B. Guseva, M. B. Berezina and A. I. Vyugin, *Inorg. Chim. Acta*, 2018, **482**, 800.
- 24 R. M. Izatt, R. E. Terry, D. P. Nelson, Y. Chan, D. J. Eatough, J. S. Bradshaw, L. D. Hansen and J. J. Christensen, *J. Am. Chem. Soc.*, 1976, **98**, 7626.
- 25 For detailed experimental and theoretical data see SI.
- 26 E. N. Nuraneeva, G. B. Guseva, E. V. Antina, O. A. Lodochnikova, D. R. Islamov and L. E. Nikitina, *Dyes Pigm.*, 2022, **201**, 110202.
- 27 W. Hu, X.-F. Zhang, X. Lu, S. Lan, D. Tian, T. Li, L. Wang, S. Zhao, M. Feng, J. Zhang and J. Lumin, *J. Lumin.*, 2018, **194**, 185.
- 28 Y. P. Rey, D. G. Abradelo, N. Santschi, C. A. Strassert and R. Gilmour, *Eur. J. Org. Chem.*, 2017, 2170.
- 29 For **1**, a reductive PET process from the benzo-15-crown-5 to the dibrominated F-BODIPY core has a negative  $\Delta G_{\text{PET}}$  value of  $-0.03$  eV according to the Rehm-Weller equation  $\Delta G_{\text{PET}} = E_{\text{ox}} - E_{\text{red}} - \Delta E_{00} - \Delta G_{\text{ion-pair}}$ .<sup>27</sup> The oxidation potential ( $E_{\text{ox}}$ ) of benzo-15-crown-5 is 1.00 V and the reduction potential ( $E_{\text{red}}$ ) of **2** is  $-1.20$  V vs. Ag/AgNO<sub>3</sub> as the reference electrode in ACN.<sup>23</sup> In ACN, the  $\Delta E_{00}$  value of **2** (533 nm) is about 2.33 eV (transition energy between the vibrationally relaxed ground and excited state of the fluorophore).<sup>23</sup> The attractive energy,  $\Delta G_{\text{ion-pair}}$  is assumed to be  $-0.1$  V.<sup>28</sup>
- 30 D. Rehm and A. Weller, *Isr. J. Chem.*, 1970, **8**, 259.
- 31 A. P. de Silva, H. Q. N. Gunaratne, J.-L. Habib-Jiwan, C. P. McCoy, T. E. Rice and J.-P. Soumillion, *Angew. Chem.*, 1995, **107**, 1889.
- 32 W. Hu, R. Zhang, X.-F. Zhang, J. Liu and L. Luo, *Spectrochim. Acta, Part A*, 2022, **272**, 120965.
- 33 X. Zhang, Z. Wang, Y. Hou, Y. Yan, J. Zhao and B. Dick, *J. Mater. Chem. C*, 2021, **9**, 11944.
- 34 M. A. Filatov, *Org. Biomol. Chem.*, 2020, **18**, 10.
- 35 P. P. Chebotaev, A. A. Buglak, A. Sheehan and M. A. Filatov, *Phys. Chem. Chem. Phys.*, 2024, **26**, 25131.
- 36 A. A. Buglak, M. O. Senge, A. Charisiadis, A. Sheehan and M. A. Filatov, *Chem. – Eur. J.*, 2021, **27**, 9934.
- 37 J. T. Buck, A. M. Boudreau, A. DeCarmine, R. W. Wilson, J. Hampsey and T. Mani, *Chem*, 2019, **5**, 138.
- 38 M. A. Filatov, T. Mikulchyk, M. Hodee, M. Dvoracek, V. N. K. Mamillapalli, A. Sheehan, C. Newman, S. M. Borisov, D. Escudero and I. Naydenova, *J. Mater. Chem. C*, 2025, **13**, 6993.
- 39 C. J. Pederson, *J. Am. Chem. Soc.*, 1967, **89**, 7017.
- 40 S. Kenmoku, Y. Urano, K. Kanda, H. Kojima, K. Kikuchi and T. Nagano, *Tetrahedron*, 2004, **60**, 11067.
- 41 Z.-J. Tan and S.-J. Chen, *Biophys. J.*, 2006, **90**, 1175.
- 42 R. D. Shannon, *Acta Cryst.*, 1976, **A32**, 751.
- 43 A. D. Becke, *J. Chem. Phys.*, 1993, **98**, 5648–5652.
- 44 C. Lee, W. Yang and R. G. Parr, *Phys. Rev. B: Condens. Matter Mater. Phys.*, 1988, **37**, 785.
- 45 F. Weigend and R. Ahlrichs, *Phys. Chem. Chem. Phys.*, 2005, **7**, 3297–3305.
- 46 F. Neese, *WIREs Comput. Mol. Sci.*, 2022, **12**, e1606.
- 47 W. Porolnik, W. Szczolko, T. Koczorowski, M. Falkowski, E. Wieczorek-Szweda and J. Piskorz, *Spectrochim. Acta, Part A*, 2024, **314**, 124188.
- 48 (a) CCDC 2457233: Experimental Crystal Structure Determination, 2025, DOI: [10.5517/ccdc.csd.cc2ngylp](https://doi.org/10.5517/ccdc.csd.cc2ngylp); (b) CCDC 2477061: Experimental Crystal Structure Determination, 2025, DOI: [10.5517/ccdc.csd.cc2p4l6n](https://doi.org/10.5517/ccdc.csd.cc2p4l6n).

